Discrete-State Representation of Ion Permeation Coupled to Fast Gating in a Model of ClC Chloride Channels: Comparison to Multi-ion Continuous Space Brownian Dynamics Simulations

Rob D. Coalson* and Mary Hongying Cheng

Department of Chemistry, University of Pittsburgh Pittsburgh, Pennsylvania 15260

Received: August 18, 2009; Revised Manuscript Received: October 7, 2009

A discrete-state model of chloride ion motion in a ClC chloride channel is constructed, following a previously developed multi-ion continuous space model of the same system (Cheng, M. H.; Mamonov, A. B.; Dukes, J. W.; Coalson, R. D. *J. Phys. Chem. B* **2007**, *111*, 5956) that included a simplistic representation of the fast gate in this channel. The reducibility of the many-body continuous space to the eight discrete-state model considered in the present work is examined in detail by performing three-dimensional Brownian dynamics simulations of each allowed state-to-state transition in order to extract the appropriate rate constant for this process, and then inserting the pairwise rate constants thereby obtained into an appropriate set of kinetic master equations. Experimental properties of interest, including the rate of Cl^- ion permeation through the open channel and the average rate of closing of the fast gate as a function of bulk Cl^- ion concentrations in the intracellular and extracellular electrolyte reservoirs are computed. Good agreement is found between the results obtained via the eight discrete-state model versus the multi-ion continuous space model, thereby encouraging continued development of the discrete-state model to include more complex behaviors observed experimentally in these channels.

I. Introduction

Discrete-state rate equation models are invoked to analyze kinetics and mechanistic details of many biological processes.[2–7] These equations typically involve first-order stepwise kinetics. That is, the instantaneous rate of transition from state i to state j is given by $k_{ij}p_i(t)$, where $p_i(t)$ is the instantaneous probability for the system to be in state i, and k_{ij} is the rate constant for transitions from state i to j. By summing the rates of gain into versus loss from state j to all other states to which it is directly linked by nonzero rate constants, the net rate of change of the probability to be in state j is established. Applying this reasoning to all N states in the system generates a set of N coupled first-order differential equations (ODEs) that prescribe its time evolution. Models of this type have great appeal for several reasons. They can describe a wide range of processes, from molecular level to subcellular to multicellular to the evolution of entire populations of organisms.[5,6,8,9] General mathematical properties of gain−loss differential equations are well understood.[10,11] Because the relevant coupled equations are linear, powerful linear algebraic methods (e.g., decomposition into eigenvalues and eigenvectors) can be applied if the number of states is not too large. In this case the dynamics can be computed out to arbitrarily long times. Furthermore, stochastic propagation methods have been devised to carry out the time evolution of systems where the number of states is too large for linear algebraic methods or direct integration of the ODEs to be effective.[12,13] In addition to the mathematical advantages just enumerated, the coupled rate equation approach has conceptual appeal. It divides the overall dynamical process into a collection of elementary steps, which can often be visualized and synthesized, mentally, in a sequential order that gives insights into the mechanism by which the process of interest transpires, including key rate limiting steps that control its time scale and character.

Despite the many virtues of discrete-state rate equation models, they are not without flaws. One problematic issue is the definition of a finite set of discrete states to represent the system's behavior in cases where the full motion of interest takes place in a very high dimensional space, often involving a continuous range of coordinates. For example, the motion of an N-atom protein takes place in continuous $3N$-dimensional configuration space. If one wishes to describe the conformational change of the protein between two locally stable configurations, one can consider the protein as a two-state system[14,15] with appropriate transition rate constants connecting these states. Whether this is a good approximation depends on the extent of fluctuations about each of these stable states, and the possible existence of locally stable intermediate states.[16] For some proteins, the nature and number of locally stable conformations may be clear, but for many it is not. Furthermore, once the relevant states that define an appropriate idealized version of the system have been identified, one still needs to know the numerical values of the rate constants that control the rate of state-to-state transitions between all pairs of states. Since the transitions involve motion in high-dimensional spaces (again, consider a protein molecule undergoing a transition between two stable conformation by passing through an unstable transition state configuration that connects them), calculating the relevant forward/backward rate constants is a nontrivial task.[17]

A class of problems where discrete-state models have long been employed, often to good effect, is in the description of the motion of ions through protein channels.[4,7,18–20] Especially if the pore of the channel is characterized by strong binding sites where ions tend to congregate, it is natural to consider a

* To whom correspondence should be addressed. E-mail: coalson@pitt.edu. Phone: 4126248261. Fax: 4126248611.

10.1021/jp907965b
Published on Web 01/05/2010

scenario where a permeant ion hops sequentially between binding sites on its way from the entrance to the exit of the channel. This idealization of the motion leads directly to a finite discrete-state model of the permeation process. Still, questions about the mapping can arise. Are the binding sites sufficiently deep that the ions spend negligible time in transit between them? Can a deep binding site accommodate only one ion at a time, or perhaps two or more? Furthermore, accurate calculation of the rate constants for hopping between internal sites, and for entrance and exit from the pore, requires considerable thought and effort.

Recently, we developed a coarse-grained computational model[1] of ion transport through a ClC chloride ion channel, and the coupling of Cl^- ion permeation to opening/closing of the fast (glutamate) gate in this channel. Compared to biological reality, the model is crude. The channel is rigid, straight (the actual permeation pathway in ClC channels is thought to be curved), and its dimensions and free energy might best be described as a caricature of features known from X-ray structure determination[21,22] and previous numerical modeling.[23–29] The glutamate gate moiety is modeled as an effective spherical particle attached to a pivot arm that can swing into and out of the channel pore. Motion is computed within a 3D Brownian dynamics (BD) framework,[30,31] involving simultaneous motion of many ions and the gate particle.

In spite of its crudeness, the model just described yielded qualitatively, and often semiquantitatively, accurate predictions for a variety of experimentally measured properties, including (i) the dependence on $[Cl^-]$, that is, Cl^- bathing solution concentration, of ion current through the open channel and (ii) the dependence of the fast gate closing rate on $[Cl^-]$. Given the existence of this computational model, which takes place in the continuous space of configurations of all ions in the simulation system plus those of the gate particle, it is of interest to attempt to reduce it to an idealized discrete-state model, and analyze the performance of such a model in comparison to the more realistic many-body, continuous motions that characterize the model just described. In fact, we have found that it is possible to successfully represent the process embodied by the many-body, continuous space model by a simplified discrete-state model that consists of three internal ion binding sites, each of which can be at most singly occupied, leading to a discrete-state model comprising eight states when the glutamate gate is open. Presentation of our analysis is organized as follows:

In Section II, we review features of the original multiparticle continuous space model, and define the reduced state space that we wish to consider in the present work. Although this state space is formally 12-dimensional when gate closing events are allowed, the essential analysis can be carried out in an 8-dimensional space, which describes ion permeation kinetics in the open channel. In this section we also briefly review essential details of the 3D Dynamic Monte Carlo (DMC) method used to carry out the BD simulations of coupled ClC gating and ion permeation that were presented in ref 1. Further simulations along these lines are carried out in the course of the present work. In addition, the same 3D DMC method is used to calculate state-to-state rate constants here. In Section III, we describe the calculation of the 24 nonzero rate constants that connect the states in the model. These calculations are done via 3D BD simulation. Most involve the motion of a single Cl^- ion. Only the rate constants that describe influx of ions from the bathing solution into the end sites of the channel pore require a multi-ion simulation. In Section IV, we review elements of kinetic master equation theory that are directly relevant to our goals. Then, in Section V, we input the numerical values of the state-to-state rate constants calculated in Section III into the gain−loss kinetic equations that describe time-evolution under the discrete eight-state model, and compute the site occupation probabilities at steady state, as well as the current-concentration curves and gate closing rates studied previously in ref 1 using the underlying multiparticle, continuous space model. Comparison between the two models is made. Finally, Section VI presents discussion and conclusions concerning the success of the reduction of this complex many-body dynamical process to a few-state system, as well as possible extensions to include other physiologically relevant components of permeation and gating in ClC channels.

II. Details of the Channel Model, a 3D DMC Method and Its Application to Ion Permeation and Gating in the ClC Channel

A. Details of the Channel Model. In ref 1 we constructed a coarse-grained model of ion permeation through a generic ClC-family channel. The model involves the 3D motion of many Na^+ and Cl^- ions in a simulation box, with a geometrically fixed impermeable channel scaffold and membrane slab. The channel geometry is based roughly on the known X-ray structure of bacterial ClC transporters.[21,22] The energetics experienced by a single ion moving through the channel (i.e., the single ion potential of mean force) is based roughly on previous computational estimates of this quantity. Coulombic ion−ion interactions are included in the model, including effects due to charge induced on the dielectric boundary between the protein channel/membrane component of the system and water solvent. Ion dynamics is then carried out assuming that the ions execute overdamped Brownian motion (i.e., in accord with a multi-ion Smoluchowski equation), which is simulated via a stochastic BD algorithm. Diffusion constant and dielectric constant profiles that influence the motion of the ions are set by comparison to profiles invoked previously in other ion channel systems[32] having similar pore sizes.

Figure 1 depicts the basic features of this model, including the effective single-ion potential of mean force (PMF) that a Cl^- ion experiences as it moves through the channel at an externally applied membrane potential of −100 mV. In all simulations conducted in this work, a −100 mV external electric potential is applied across the membrane, which drives a Cl^- ion from the internal to the external solution. The presumed fast gate E166 in the ClC-0 channel (homologous to E148 in the StClC transporter) is modeled as a spherical particle attached to a lever whose pivot is located in the wall of the pore. This gate particle moves in a bistable potential, which varies with the angle of its lever arm with respect to an appropriate reference orientation: one stable state (potential minimum) corresponds to the situation where the gate particle occupies the S_{ext} binding site (thus preventing a Cl^- ion from occupying the same site); the other stable state corresponds to the gate particle being pinned back away from the channel pore (so that Cl^- ions can permeate through the channel). These two stable states are separated by a significant energy barrier, so that the transition from one stable state to the other (opening and closing of the glutamate gate) is an activated process (cf. Figure 2 of ref 1).

In the top panel of Figure 1, which shows the PMF experienced by a single Cl^- ion as it moves through the channel when an uncharged gate particle is in its open state configuration (again, pinned back away from the pore), three deep potential energy wells are apparent, corresponding to internal ion binding sites S_{int}, S_{cen}, and S_{ext} identified in the X-ray structure of bacterial ClC transporters.[21,22] (The energetic stability of these

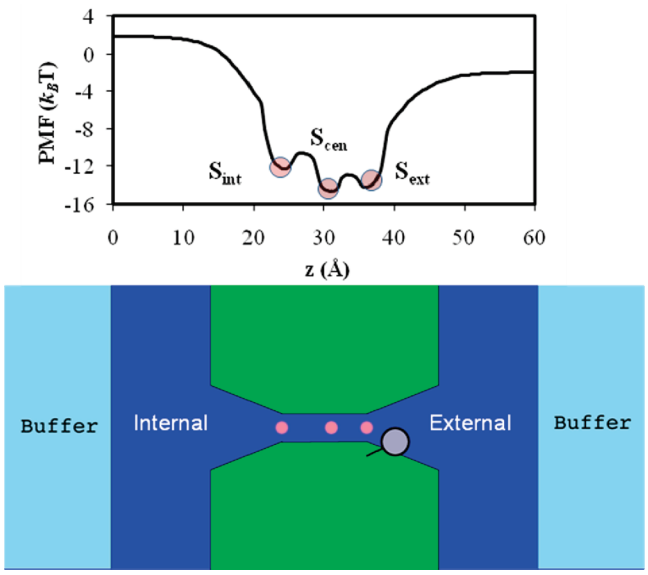

Figure 1. 3D ClC channel model, showing location of three Cl^- binding sites and the effective single-ion PMF that a Cl^- ion experiences as it moves through the open channel at an applied external potential of −100 mV. Opening/closing of the fast (glutamate) gate is modeled via a spherical particle attached to a pivot rod, as indicated in the lower panel. The locations of the three Cl^- binding sites are marked by small pink circles in this panel.

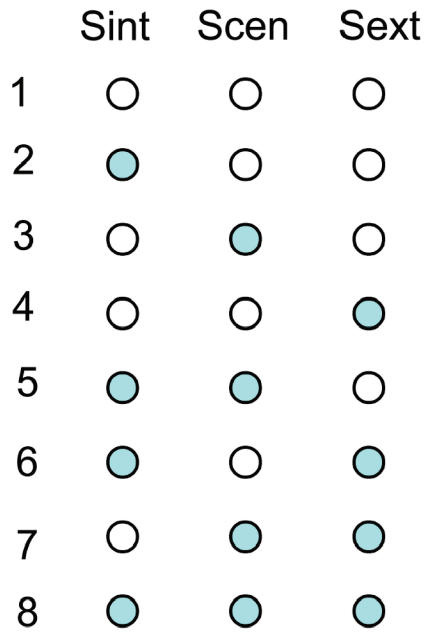

Figure 2. Eight discrete states accessible when the channel is open. Note that each binding site is either empty or occupied by a single Cl^- ion (multiple site occupancy is not allowed).

sites is conferred by their proximity to critical amino acids lining the pore. See ref 22 for details.) The depth of the binding sites suggests a site model of the ion permeation kinetics:[19,20] an ion in the channel can occupy one of these sites within the channel. It can then hop to another site, although no site can accommodate more than one ion. (The maximum single occupancy paradigm is supported by X-ray structures of bacterial ClC transporters,[21,22] which show no more than one Cl^- ion in any of the three intrapore binding sites. This is not unexpected given that the pore is so narrow that Cl^- ions must traverse it in single file.) We are thus led to the eight-state kinetic model for motion through the open channel indicated in Figure 2. Since in our 3D BD simulations ions move in continuous space, we will define "occupation" of a site by an ion by setting up a position window centered on that site. Of course, the size of the window is somewhat arbitrary, thus illustrating one of the difficulties in constructing a precise map of the multi-ion continuum space motion to a finite set of discrete states. This point will be discussed further in Section V.

Transitions between the eight states are allowed with appropriate restrictions. In particular, only transitions between adjacent sites are allowed, while transitions that would entail hops spanning two or more sites are forbidden. For example, the rate constant k_{23}, which describes transitions between states 2 and 3, corresponding to a hop from S_{int} to S_{cen} (cf. the state diagram Figure 2), is generally nonzero, that is, the process is allowed. By contrast, k_{24}, corresponding to a direct hop from S_{int} to S_{ext}, is zero, that is, the process is disallowed. Note that the same rule applies to ion entry and exit from the channel. An ion can enter from the internal reservoir, effectively "jumping" from the reservoir to S_{int}, so k_{12} is generally nonzero. However, the ion cannot jump from the reservoir directly to S_{cen}, so k_{13} is identically zero. These rules imply a total of 24 nonzero rate constants for this 8-state model of ion permeation in the open channel.

Given the discrete-state space, there remains the issue of how to compute state-to-state rate constants. In systems where the reduction to a discrete-state space is extremely coarse-grained or idealized, even the formulation of a precise strategy for rigorous computation of rate constants may be elusive. However, in the case under study here, the appropriate procedures are reasonably straightforward. The transitions fall into three types: (i) hops between adjacent sites in the channel, (ii) escape from one of the end sites into the corresponding bulk reservoir, and (iii) entrance from a bulk reservoir into the nearest Cl^- binding site within the channel pore. The first two types of transitions are single-particle processes. The most straightforward way to calculate the relevant rate constants is to simulate them using our 3D BD algorithm to compute the stochastic motion of a single ion. Details will be provided in Section III. The third class, influx from a bulk reservoir into an adjacent binding site inside the channel, requires simulation of the motion of many ions in the reservoir. At very low bulk (bathing solution) ion concentrations the motion of these ions is independent, and therefore, in principle, only the motion of a single representative ion would need to be considered. In this limit, the steady-state rate of absorption of ions at the relevant binding site is strictly proportion to the ion concentration in the bulk reservoir.[33] However, as the reservoir ion concentration increases, ion−ion interactions affect the rate of influx into the channel: in particular, ion−ion repulsions lead to a saturation effect, such that increasing the ionic strength in the reservoir does not result in a higher influx rate into the channel. Again, full computational details of the state-to-state rate constant calculations are provided in Section III.

B. 3D DMC Algorithm for Simulation of Many-Particle Brownian Dynamics. Here we briefly review the details of the 3D DMC technique which we utilized in ref 1 to carry out multi-ion BD simulations coupled to a 1D gate particle coordinate as schematized in Figure 1.

We utilized a DMC algorithm[30,31] to stochastically simulate Brownian motion of a system of a collection of spherical ions in the high friction limit. The numbers of ions in the left (intracellular or "internal") and right (extracellular or "external") buffer regions, N_L and N_R, respectively, are held fixed. This is done by integrating the prescribed bulk ion concentrations C_L and C_R over the volumes of the buffer (the light blue regions in

Figure 1); buffer region ions are distributed randomly at each Monte Carlo (MC) cycle to maintain a constant concentration boundary condition. (Note: the desired cation and anion concentrations are individually maintained.) The number of ions N_I in the channel/vestibule regions (dark blue region in Figure 1) fluctuates over the course of the simulation. Hence, in order to maintain proportionality between a cycle of MC moves and a step in real time, we introduce N_v "virtual particles" into the system. These particles are not actually moved, but serve as place holders which, again, ensure the proportionality between a cycle of MC moves and a step in real time. Specifically, the number of virtual particles varies in the course of the simulation such that $N = N_L + N_R + N_I + N_v$ (the number of real particles plus the number of virtual particles in the simulation) remains constant. An MC cycle then consists of N random selections of one of the N total particles in the system. (Thus, each real particle is moved on average one time during one MC cycle.) If a real particle is chosen, it is stochastically updated as described below; if a virtual particle is chosen, nothing further is done.

For example, consider a DMC simulation that involves a constant concentration of 0.135 M NaCl for both internal and external bulk solutions. Assuming a buffer region of 40 × 40 × 30 Å on each side, we randomly distribute $N_L = N_R = 4$ (2 for Cl^- and 2 for Na^+ to make the buffer neutral) at each MC cycle to implement a constant concentration of 0.135 M. For a simulation system of 40 × 40 × 60 Å, we choose $N_I = 8$ and $N_v = 2$ for the initial configuration. Thus, the total number of ions used is $N = 18$. Again, N_I varies with the simulation time and N_v changes accordingly so as to maintain a constant number of N. In practice, N_v is initially chosen to be 20−30% of N_I.

One MC cycle consists of N steps. At each step, one ion k is randomly chosen and moves $\pm h_z$ in one direction (x, y, or z), if it is not a virtual ion. The ion displacement size h_z is assumed to be dependent on its position along the channel axis (z direction) only and is related to the local ion diffusivity $D(z)$ according to $h_z^2/D(z) = h_0^2/D_0$, where h_0 and D_0 are the ion displacement and diffusivity in the bulk, respectively. The new configuration is accepted if Rand < $\exp(-\beta\Delta W_k)$, where Rand is a uniform random number on the interval [0, 1] and $\beta = (k_B T)^{-1}$; the energy determining the configuration change is given by

$$W_k = \phi_k^{\text{stat}} + \sum_{j\neq k} \frac{q_k q_j}{\varepsilon_w}\phi^{\text{coul}}(r_{kj}) + \sum_{j\neq k} q_k q_j \phi_{kj}^{\text{diel}} + \frac{q_k q_g}{\varepsilon_w}\phi^{\text{coul}}(r_{kg}) + q_k q_g \phi_{kg}^{\text{diel}} - k_B T \ln(D(z)/D_0) \quad (1)$$

where q_k, q_j, and q_g are the charges of the chosen ion k, other nonvirtual ions j, and the gate particle, respectively. The first term on the right-hand side of eq 1 is the PMF to transport a single ion through an empty channel with a neutralized E166 residue (homologous to E148 in StClC transporter). This PMF function is shown for the Cl^- ion species in the upper panel of Figure 1. For Na^+, the corresponding PMF features a high barrier (not shown here) in the channel region (cf., Figure 3 of ref 1) that effectively prevents Na^+ ions from entering the channel. The second and third terms account for Coulombic interactions between the chosen ion k and other ions. A detailed description of these terms is given in refs 30 and 31. Briefly, the term $\phi^{\text{coul}}(r_{kj})$ is a truncated Coulomb potential,[30] while the term ϕ_{kj}^{diel} accounts for the fact that our simulation system is dielectrically inhomogeneous: the dielectric constant of the aqueous regions (both inside and outside the pore region) is

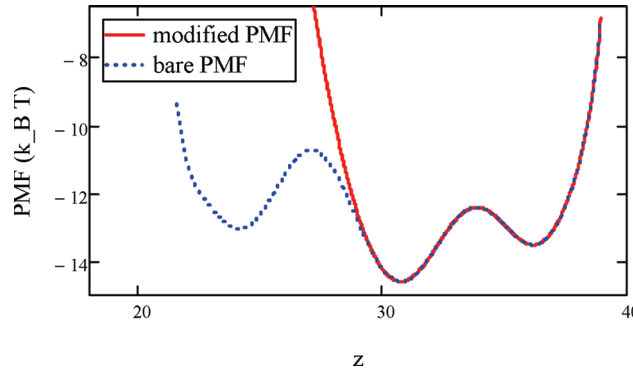

Figure 3. Dashed blue line shows "bare" single-ion PMF for Cl^-. Solid red line shows a modified PMF, where a quadratic function based on Taylor's series expansion about the minimum of the S_{cen} well has been spliced on to the left-hand side of the S_{cen} well. This prevents an ion placed initially in S_{cen} from exiting to the left (i.e., into S_{int}).

taken to be $\varepsilon_w = 80$, while the dielectric constant in the membrane/protein regions is taken as $\varepsilon_p = 20$. In fact, we have found in previous work[34] that to a good level of approximation ϕ_{kj}^{diel} is determined by the individual dielectric self-energies of inserting ions k and j into the channel. These self-energies can be calculated by solving the 3D Poisson equation for the dielectric configuration relevant to our ion channel problem.[30,34,35] The fourth and fifth terms correspond in a similar fashion to Coulombic interactions between the gate particle and the chosen ion k. The last term accounts for the effect of a nonuniform ion diffusion constant profile that varies along the channel direction.[31]

The gate particle is modeled as a sphere attached to a rod and is assumed to undergo 1D angular motion around a pivot fixed near S_{ext}. It is updated once in each MC cycle. In one MC step, the gate attempts to move through an angle $\pm\Delta$. This new configuration is accepted if Rand < $\exp(-\beta\Delta W_g)$, where ΔW_g is the energy change of the gate particle between these two configurations. The energy of the gate is calculated as follows:

$$W_g = \phi_g(\theta) + \sum_j \frac{q_g q_j}{\varepsilon_w}\phi^{\text{coul}}(r_{gj}) + \sum_j q_g q_j \phi_{gj}^{\text{diel}} \quad (2)$$

where θ is the angle of the pivot rod connecting the gate particle to the channel with respect to an appropriate reference configuration. $\phi_g(\theta)$ is a bistable potential representing the angle-dependent intrinsic gate potential energy, whose two minima correspond to the gate in the open and closed configurations, as noted above (cf. Figure 2 of ref 1). The second and third terms on the rhs of eq 2 account for Coulombic interactions between the gate particle and the ions. The gate particle angular step size Δ is related to the effective diffusion constant assigned to the particle so as to properly synchronize it with the ions' motion.[1] The total simulation time T_s is related to the total number of MC cycles N_c as

$$T_s = \frac{h_0^2 N_c}{6D_0} \quad (3)$$

In addition to the electrostatic potential terms outlined above, a hard-core excluded volume potential is included in our simulations to prevent overlap between an ion and the protein/membrane, between any two ions, or between ions and the gate particle. In particular, any movement generating such an overlap is not allowed. The radius of the Cl^- ion is taken to be 1.8 Å, and that of the Na^+ ion is taken to be 0.95 Å. The gate particle sphere is assigned a radius of 2.0 Å in order to roughly mimic

the size of the glutamate side-chain that it represents. In the present work, the gate particle is assumed to be neutral, which corresponds to a protonated E166 residue in the open ClC-0 channel (following experimental evidence suggesting that the glutamate gate must be protonated in order to open[22,36,37]). Thus, Coulombic interactions between the gate particle and ions in eqs 1 and 2 are set to be zero (i.e., $q_g = 0$). (Note that the gate particle *does* interact with the permeant ions via the excluded volume interactions described above.)

III. Calculation of State-to-State Rate Constants via 3D DMC Simulation

Here we describe how the same simulation technique, with the gate particle frozen in its "open" position, can be used to extract state-to-state rate constants for the discrete-state model considered in the present work. As in our previous 3D DMC simulations of this system, the simulation box (excluding the buffer regions) has a size of $L_x \times L_y \times L_z = 40 \times 40 \times 60$ Å. The DMC displacement step for ions in the bulk is set to 0.5 Å in all kinetic rate constant calculations. The diffusion profile along the channel direction is taken to be the same as in our previous study.[1] As noted above, three generic types of state-to-state transition need to be considered, namely (i) hops from one binding site to an adjacent one, (ii) escape from one of the terminal sites of the channel into the abutting bulk reservoir, and (iii) entry from bulk reservoirs into the adjacent end site within the channel. Each case will be considered in turn.

A. Site-to-Site Hopping. As a specific example, consider the case of transitions between states 3 and 4 corresponding to a hop from S_{cen} to S_{ext}, that is, the rate constant k_{34}. We place a single Cl^- ion in the single ion PMF well (cf., Figure 1) corresponding to the binding site at S_{cen}. We then allow it to move in 3D via our DMC algorithm. (Note: Since our system consists of a single ion here, complications associated with a time-varying number of ions described in Section IIB do not occur. The same remark holds for the escape of an ion from an exterior binding site into the abutting bulk reservoir, which will be considered in Section IIIB below.) Our goal is to calculate the average time it takes for the ion to make a transition to the S_{ext} well, which we define as the first time that the ion reaches the minimum of the S_{ext} well. Note that if we simply track the motion of the ion via 3D DMC simulation, there is some possibility that it will hop in the opposite direction, in this case to the S_{int} binding site. To suppress this possibility, we modify the single-ion PMF profile as follows. We replace the left half of the S_{cen} PMF well (i.e., to the left of the minimum of this well) with a quadratic potential that has the same minimum and the same curvature at the minimum, as depicted in Figure 3. Now the ion is naturally confined to S_{cen} until it makes a transition to S_{ext}. The mean first passage time τ_{34} from the equilibrium position of S_{cen} to that of S_{ext} under the modified potential is computed by repeating the stochastic DMC simulation for 1000 runs: then $k_{34} = 1/\tau_{34}$. In the present study, all state-to-state rate constants are averaged over ca. 800−1000 individual runs. We found that at least 100 individual runs are necessary for good statistics. A similar PMF modification is performed for all rate constant calculations involving hops between two adjacent binding sites and for escape from an external binding site to the abutting reservoir: viz., the "wrong way" escape route is blocked by replacing the actual PMF curve with one where the potential in the "wrong direction" is a grafted quadratic and hence naturally prevents wrong-way escape.

An ion can also hop from S_{cen} to S_{ext} while there is another ion occupying the S_{int} site. This is represented by a transition

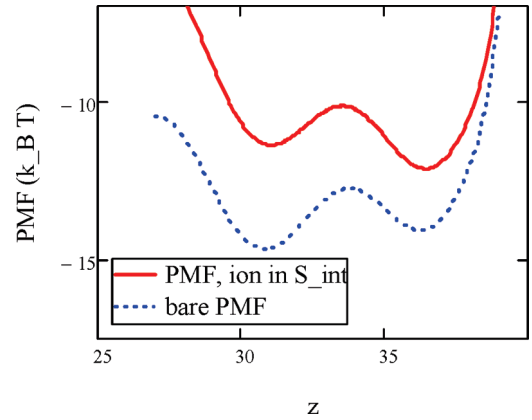

Figure 4. An ion pinned in S_{int} generates the modified single-ion PMF (red line) in the $S_{cen}-S_{ext}$ region of the channel. "Bare" PMF (no ion in S_{int}) is shown by a dashed blue line.

from state 5 to 6 in our discrete-state model. The hopping process still involves only one particle, but the effective potential (free energy profile) that the particle experiences is modified by additional Coulomb interactions of the hopping ion with the ion "pinned" in S_{int}: cf. Figure 4. The additional Coulomb interaction between the hopping ion k and the ion j bound to S_{int} is calculated, as noted above, using an empirical ion−ion interaction potential:[34]

$$\phi_{kj}^{\text{int}} = \frac{q_k q_j}{\varepsilon_w}\phi^{\text{coul}}(r_{kj}) + 2q_k q_j\sqrt{\phi_{k\leftarrow k}^{\text{diel}}\phi_{j\leftarrow j}^{\text{diel}}}\exp(-cr_{kj}/L) \quad (4)$$

where $\phi_{k\leftarrow k}^{\text{diel}}$ and $\phi_{j\leftarrow j}^{\text{diel}}$ are the dielectric self-energy (i.e., the image potential) for the hopping ion k and "pinned" ion j, if each has a unit (proton) charge. (We are specifically considering Cl^- ions here, so that $q_k q_j = 1$ in eq 4.) A detailed description of how self-energy is calculated for an ion inside a channel pore may be found in ref 34. In the second term in eq 4, L is the length of the channel, r_{kj} is the distance between the ions k and j, and $c = 2.0$. In the present study, $L = 30$Å; furthermore, the dielectric self-energy for an ion located at S_{int}, S_{cen}, and S_{ext} is found numerically to be $\phi_{S_{int}}^{\text{diel}} = 1.7k_BT$, $\phi_{S_{cen}}^{\text{diel}} = 2.1k_BT$, and $\phi_{S_{ext}}^{\text{diel}} = 1.7k_BT$, respectively.

To calculate the rate constant k_{56}, we repeat the 3D DMC simulation procedure used to calculate k_{34}, substituting the modified effective potential energy profile depicted in Figure 4. Due to the strength of Coulombic forces on this atomic distance scale, the presence of an ion in a nearby binding site can substantially perturb the PMF experienced by a hopping ion. In particular, the height of the energy barrier separating initial and final wells relevant to the hopping process can change by several k_BT with respect to the location of the minimum of the potential well that corresponds to the initial state, thus significantly changing the hopping rate. The underlying theory describing such processes will be briefly reviewed in Section VI. (Note that we repeated the same 3D BD simulation calculation of k_{56}, allowing the ion in the S_{int} site to fluctuate in the S_{int} potential well rather than fixing its location at the minimum of the well. Such fluctuations were found to have no significant influence on the extracted rate constant.)

To summarize, site-to-site hopping is inherently a single ion process. Thus, the site-to-site rate constants are independent of the concentration of Cl^- ions in the abutting bulk reservoirs. These rate constants *do* depend on the single ion PMF and the Cl^- ion diffusivity profile, a point which is discussed in more quantitative detail in Section VI below. For example, a change

in applied voltage across the membrane will change the single ion PMF, and thus all site-to-site hopping rate constants.

B. Escape to the Bulk Solution from an Exterior Binding Site. The basic computational procedure here is the same as for site-to-site hopping. For example, consider a Cl^- ion that initially occupies the S_{int} binding site and eventually escapes to the intracellular reservoir. To compute the rate constant for this escape process based on the model of ion permeation introduced in ref 1, we place at $t = 0$ one ion in S_{int}, replace the PMF to the right of the equilibrium position of the S_{int} well with a locally matched quadratic function (to prevent a transition to the S_{cen} well), and then perform DMC simulation and record the time it takes for the ion to exit the vestibule. This process is repeated 1000 times, until the mean first passage time for escape to the intracellular vestibule is accurately established. Again, the inverse of the mean first passage time is the rate constant k_{21}. Similar calculations are performed to determine the analogous rate constants when another ion occupies S_{cen} and/or S_{ext}, in each case modifying the effective single-ion PMF in accordance with the additional Coulombic repulsions experienced by the mobile channel-exiting ion due to the presence of other fixed ions in the channel. Finally, the same suite of simulations is carried out to establish rates of escape from S_{ext} to the extracellular reservoir. Note that just as in the case of site-to-site hopping, escape of an ion from the channel pore into the abutting bulk solvent region is a single particle process. The corresponding rate constants are thus independent of the concentration of Cl^- in the reservoirs, but they do vary when either the single ion PMF of the ion diffusivity profile is modified.

C. Influx from the Bulk Solution to an Interior Binding Site. This is the inverse process to that treated in the preceding subsection. However, calculation of the influx rate constants requires a somewhat different simulation strategy than calculation of the corresponding efflux rate constants. For example, to calculate k_{12}, we start with a multi-ion bulk reservoir corresponding to a specified bath concentration with all ions interacting via the relevant Coulomb and excluded volume forces. We then perform 3D DMC simulation of all ions in the bulk reservoir and impose an absorbing boundary condition at the location of the S_{int} binding site; additional ions are inserted randomly into the bulk reservoir in order to maintain the desired bulk ionic strength. A steady state situation is thus generated, and we can numerically determine the rate at which Cl^- ions are absorbed at the sink imposed at the S_{int} binding site. (As noted above, due to the different single ion PMFs seen by Cl^- and Na^+, the Na^+ ions do not actually enter the channel from the bulk.) In the absence of ion−ion interactions, we would expect the rate of Cl^- ion absorption at the imposed sink to scale proportionally to the bulk ion concentration of Cl^-. In our simulations, we observe this behavior at low ionic strength. However, at higher ionic strengths (approaching 1 M) this rate begins to saturate to a maximum value. We trace this behavior primarily to ion−ion Coulombic interactions. Compared with ion−ion Coulombic interactions, hard-sphere repulsion (ion–ion excluded volume effects) has a much smaller effect on k_{12}: cf. Figure 5. As more Cl^- ions are drawn into the vestibule, they generate additional repulsive forces acting on further Cl^- ions that try to enter from the bulk, eventually making it impossible to drive more ions into the vestibule region no matter how high the bulk Cl^- ion concentration is. An example of this behavior is shown in Figure 5 for the case of ion influx from the intracellular reservoir into the S_{int} binding site with no other ions in the channel, that is, the transition from state 1 to state

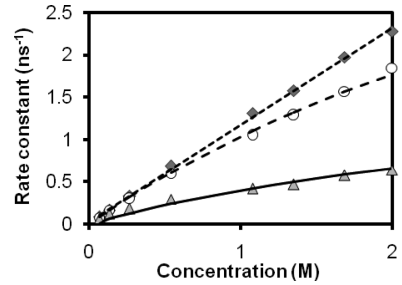

Figure 5. Comparison of internal concentration dependence of rate constant k_{12}. Filled triangles show results of 3D multi-ion BD simulation results. Solid line represents Michaelis−Menten type functional fit to this data. (Fit parameters are given in Table 1). Diamonds show rate constants obtained assuming no Coulombic interactions with overlap between ions allowed (i.e., excluded volume interactions are turned off), and the dotted line represents a linear fit to the simulation data points. Circles indicate rate constants assuming no Coulombic interactions with no overlap allowed between ions (i.e., excluded volume interactions are turned on), and the dashed line shows Michaelis−Menten type functional fit to these data points. Each data point is an average based on 800−1000 simulation runs, with the error bars on the mean value being ±5−10%.

TABLE 1: Numerically Simulated State-to-State Rate Constants for the Eight-State Model[a]

forward rate consts.	K_{max}	Cl_s	reverse rate consts.	
k_{12}	2.1	4.0	k_{21}	0.000 41
k_{14}	0.52	1.5	k_{41}	0.0017
k_{23}	0.56		k_{32}	0.041
k_{26}	0.50	3.2	k_{62}	0.0021
k_{34}	0.52		k_{43}	0.69
k_{35}	1.0	5.0	k_{53}	0.0032
k_{37}	0.39	4.0	k_{73}	0.015
k_{46}	1.33	4.6	k_{64}	0.0014
k_{56}	0.98		k_{65}	0.40
k_{58}	0.25	5.0	k_{85}	0.040
k_{67}	0.31		k_{76}	0.14
k_{78}	0.75	6.0	k_{87}	0.0092

[a] For the influx processes, the values of the parameters K_{max} and Cl_s which define rate constant fits based on eq 5 are provided. All rate constants are given in ns^{-1} and all concentrations are in M = mol/L.

2. The numerically computed dependence of k_{12} on the internal Cl^- concentration is found to be well represented by a 2 parameter function of Michaelis−Menten form; generically,

$$k = K_{max}/(1 + Cl_s/[Cl^-]) \quad (5)$$

where K_{max} is the saturation rate constant in units of ns^{-1} and Cl_s is the concentration at which half of the saturation rate constant is attained. Both Cl_s and $[Cl^-]$ are in units of molarity M. A similar analysis was carried out for variants of this situation where an ion is bound in the S_{cen} and/or S_{ext} sites, and for the analogous processes involving influx from the external reservoir.

The results of this 3D BD simulation based analysis are presented in Table 1. Rate constants for site-to-site hopping transitions and for terminal binding site to bulk reservoir efflux transitions are given in units of ns^{-1}. For influx processes, we specify K_{max} in ns^{-1} and Cl_s in M. The numerical values of K_{max} and Cl_s that appear in Table 1 are simply intended to give a reasonable global fit to the corresponding 3D BD data on the concentration interval $0 < [Cl^-] < 2$ M: there may exist other values of these parameters that yield fits of similar quality. Obviously, in contrast to the rate constants that characterize site-to-site hopping and efflux of an ion from a channel binding

site to the abutting bulk reservoir, the rate constants describing influx of Cl^- ions from a bulk reservoir into the nearest binding site inside the channel are manifestly dependent on the concentration of Cl^- ions in the reservoir. (Of course, these influx rate constants are also dependent on the single chloride ion PMF and its spatial diffusivity profile.)

IV. Analysis of Kinetics According to the Discrete State Model

Let $p_i(t)$ be the probability to find the ion channel system in state i. Then the time evolution of the state occupation probabilities of the N states in the system is given by the following set of kinetic master equations:

$$dp_i(t)/dt = \sum_{j=1}^{N} [k_{ji}p_j(t) - k_{ij}p_i(t)]; \quad i = 1 - N \qquad (6)$$

where $k_{ii} = 0$, $i = 1 - N$, by construction. For each state i, $\sum_{j=1}^{N} k_{ji}p_j(t)$ gives the rate at which the probability in state i increases due to transitions from all directly connected states j, while $-\sum_{j=1}^{N} k_{ij}p_i(t)$ gives the rate of loss from state i due to transitions to all directly connected states j. In the present problem we are interested in the flow of probability between the $N = 8$ states of our open channel discrete-state model. Of primary concern is the steady state probability distribution attained after short-time transient decay. These steady state populations obviously depend on the numerical values of the rate constants in the model. The principal experimentally adjustable parameters are the voltage applied across the membrane and the concentrations of ions in the bathing solutions. Changing the voltage drop across the channel changes the single ion PMF for a Cl^- ion in the channel, and thus all the nonzero rate constants for state-to-state transitions in our discrete-state model. Changing the ionic strength of one of the reservoirs changes the rate constants for the state to state transitions which correspond to injection ("influx") of an ion into the corresponding exterior binding site within the channel pore, as discussed in Section IIIC.

Let us write the N linear equations in eq 6 in the matrix/vector form $\dot{\vec{p}}, = \mathbf{w}\vec{p}(t)$, where $\mathbf{w}$ is the appropriate 8×8 matrix of conditional transition probabilities. The eigenvalues and eigenvectors of $\mathbf{w}$ can easily be computed using standard procedures of numerical analysis. Designating the 8×8 matrix of eigenvectors (one eigenvector in each column of the matrix) as $\mathbf{T}$, then if the inverse of $\mathbf{T}$ exists we can decompose $\mathbf{w}$ as $\mathbf{w} = \mathbf{T}^{-1}\Lambda\mathbf{T}$, where Λ is the diagonal matrix of eigenvalues of $\mathbf{w}$. Because $\mathbf{w}$ is not generally a symmetric matrix, it is difficult to prove mathematically that $\mathbf{T}^{-1}$ exists for arbitrary values of the underlying state-to-state rate constants. However, for all cases that we have examined numerically, we have found upon applying a standard Gauss-Jordan elimination procedure that $\mathbf{T}^{-1}$ *does* exist. Once $\mathbf{T}^{-1}$ has been constructed, it is straightforward to compute the matrix $\exp(\mathbf{w}t)$ and hence to propagate any initial vector of state probabilities to any desired time. Furthermore, we have found numerically for all cases studied that there is a single eigenvector corresponding to eigenvalue 0, and all other eigenvalues have a real part that is less than 0. Given these properties of $\mathbf{w}$, then any initial state probability vector normalized to 1 (i.e., such that the sum of all components is unity) will evolve to the long time limit $\vec{p}(\infty) = \vec{\tilde{p}}$, where $\vec{\tilde{p}}$ is the unique eigenvector corresponding to eigenvalue 0 (normalized so that its components sum to 1). Since we are only interested here in the steady state properties of this system, all the information we need is contained in this particular eigenvector of $\mathbf{w}$.

Given the steady state occupation probabilities of all the states, that is, the vector $\vec{\tilde{p}}$ identified above, then both the current of ions through the open channel and the average gate open time or, equivalently, gate closing rate in the channel can easily be computed for our eight-state model of the open ClC channel. Calculating the rate of current flow through the open channel is straightforward. The net (particle) current of Cl^- ions through the channel is given by $J = J_{\rightarrow} - J_{\leftarrow}$, where $J_{\rightarrow}$ is the rate at which Cl^- ions make transitions from the S_{cen} to the S_{ext} binding site and $J_{\leftarrow}$ is the rate at which Cl^- ions make transitions from the S_{ext} to the S_{cen} binding site. [Note: The same result for the net rate of flow of ions through the channel would be obtained by focusing on any other link in the kinetic pathway.] Since each Cl^- ion carries an electric charge of $-e_0$, e_0 being the proton charge, the total electric current flowing through the channel is $I = -e_0J$. In terms of the steady-state probability distributions of the eight states in open ClC channel model:

$$J_{\rightarrow} = k_{34}\tilde{p}_3 + k_{56}\tilde{p}_5, \quad J_{\leftarrow} = k_{43}\tilde{p}_4 + k_{65}\tilde{p}_6 \qquad (7)$$

Calculating the closing rate of the fast gate via explicit multiparticle simulation of both the gate particle motion and that of mobile ions in the channel and reservoirs is extremely challenging. The experimentally observed time scales of gate closing are on the order of milliseconds. Thus, even when the gate motion is represented as that of an effective spherical particle on a pivot rod (cf. Figure 1) and the applicability of BD is assumed, the number of time steps required to carry out the desired simulation with experimentally relevant gate-closing rates (controlled in the simulation model of ref 1 via the barrier height of the gate particle potential and the gate particle diffusion constant) is prohibitively long. Hence, in the multibody gate closing simulations performed in ref 1 we reduced the barrier height and/or increased the diffusion constant governing the gate particle motion along its 1D pivot rod angular coordinate so as to reduce the time scale of gate closing to 0.1−1 microseconds, which *was* accessible via explicit BD simulations. Fortunately, we found within the range of gate potential energy parameters which we could explicitly treat in this fashion (the height of the barrier in the potential function $\phi_g(\theta)$ being of particular importance) that the average gate-open time (inverse to the gate-closing rate) scaled proportionally to the time of gate-closing extracted from the BD of the 1D gate particle coordinate *in the absence* of Cl^- ions moving through the channel pore. Moreover, designating the average gate-open time (or, equivalently, the average time for an initially open gate to close) extracted for the bare gate-particle motion as τ_0, then the average gate-open time obtained from full multi-ion simulations at fixed external reservoir chloride concentration was found to vary with the internal reservoir chloride ion concentration, c, as

$$\tau(c) \cong \tau_0/(1 - f_{occ}(c)) \qquad (8)$$

where $f_{occ}(c)$ is the average fractional occupation of the S_{ext} site by a Cl^- ion when the channel is *open* (which we determined in ref 1 via multi-ion BD simulation). This analysis, inspired by the "foot in the door" mechanism of Chen et al.,[38,39] is consistent with and partially presaged the injunction of a discrete-state model to describe coupled ion permeation and gate closing in this ion channel system. Given the applicability of eq 8, we can anticipate the effect of raising the angular PMF barrier or lowering the effective gate-particle diffusion constant: this will simply change τ_0 by an amount which can be calculated by appealing to the 1D Kramers formula.[1] Thus, even though

we cannot simulate the experimentally relevant time scale directly via a stochastic BD algorithm, we can predict the experimentally relevant average gate-open time via eq 8 (by adopting appropriate gate-particle PMF and diffusion constant).

A firmer conceptual foundation for eq 8 was subsequently developed[3] in the context of a highly simplified two-binding site model of a "ClC-like" channel system. In ref. 3 the following insight was provided: The closing rate of the bare gate particle coordinate is several orders of magnitude slower than the rate of ion permeation through the open channel. Hence, in calculating the survival probability of the gate-open state of the channel, the distribution of probability among the various open-channel substates is instantaneously balanced in proportion to the steady-state probabilities associated with the open-channel system (i.e., in the absence of gate-closing complications). The instantaneous establishment of steady state relative probabilities within the open channel manifold of substates (which differ among themselves with respect to the occupation of Cl^- in the binding sites of the pore) leads directly to a survival probability of the gate-open conformation of the channel having the form $\exp(-t/\tau(c))$, where $\tau(c)$ depends on the steady-state occupation probabilities of the open-channel system (represented by eight states in our model), and the state-to-state transition rates for each type of gate closure event. In the present model there are four closed-gate states, each with the gate-particle occupying the S_{ext} binding site and the sites S_{int} and S_{cen} either empty or singly occupied. Since we are considering only an uncharged gate (corresponding to a protonated glutamate E166 residue) here, these four gate-closing transition probabilities are equal, each being given as τ_0^{-1}. Alternatively stated, the gate-closing transition probability is independent of whether S_{int} and/or S_{cen} are occupied by a Cl^- ion. Under such circumstances $\tau(c)$ is specified as in eq 8, with $f_{occ}(c)$ given in the case of the present eight-state model of the open configuration of the ClC channel by the relevant sum of steady-state occupation probabilities,[3] namely

$$f_{occ}(c) = \tilde{p}_4 + \tilde{p}_6 + \tilde{p}_7 + \tilde{p}_8 \qquad (9)$$

V. Comparison of Discrete-State Model Kinetics to Results from the Multi-Ion Continuum BD Model

As has already been noted, the fundamental outputs of the discrete-state model developed above are the steady state populations of the eight states of the model. Fixing the applied voltage at −100 mV and the external Cl^- concentration at the value 0.135M, we can scan the results for state populations as a function of internal Cl^- concentration. This generates the data necessary to extract both the average gate open time and the ion current through the open channel. In Figure 6 we show the results for selected state populations as a function of $[Cl^-]_{int}$ (all other parameters being fixed) obtained from the discrete-state model and 3D BD multi-ion simulations using the continuous space model of ref 1. Within the context of the latter model, we define a site to be occupied if an ion is in a spatial window of ±2.5 Å about the center of the site (local minimum in the single ion PMF). Thus, at each time step of the multi-ion BD simulation, we determine if the S_{int}, S_{cen}, and/or the S_{ext} sites are occupied using the "window" definition above. If any or several of these sites are occupied, the system is said to be in one of the states 2−8 (cf. Figure 2). If none of these three sites is occupied, we assign the system to state 1 (no ions in the channel). The agreement between the predictions of the discrete-state model (solid lines) and the multi-ion continuous model (filled diamond symbols) is seen to be rather good,

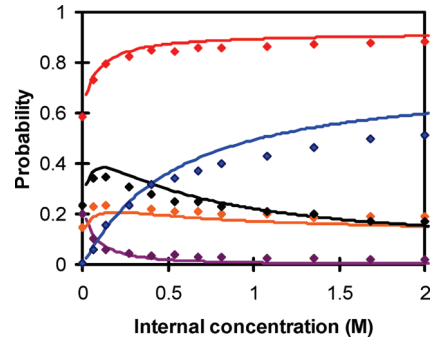

Figure 6. Steady-state occupation probabilities for state 4 (purple), state 6 (orange), state 7 (black), state 8 (blue), and the total Cl^- occupation probability at S_{ext} (the sum of these four probabilities, shown in red), as a function of $[Cl^-]_{int}$, at fixed $[Cl^-]_{ext} = 0.135$ M. Solid lines represent results obtained using the 8-state discrete model and filled diamonds represent results from the 3D BD model. The error bars for the BD simulation data points are ±5−10%.

especially considering the obvious difficulties involved in mapping the many-body dynamical system into one described by eight discrete states. All the qualitative features predicted by the eight-state model are consistent with the simulated dynamics of the multi-ion continuous space. Indeed, the agreement is nearly quantitative. One particularly important quantity is the sum $\tilde{p}_4 + \tilde{p}_6 + \tilde{p}_7 + \tilde{p}_8 = f_{occ}$, which is the total probability to find the system in a state with S_{ext} occupied by a Cl^- ion. This effectively determines the gate closing rate in the discrete-state model, as discussed above. At the external reservoir Cl^- concentration $[Cl^-]_{ext} = 0.135$ M, then at internal reservoir concentration $[Cl^-]_{int} = 0$ M $f_{occ} \cong 0.6$, while for large $[Cl^-]_{int}$ (say, $[Cl^-]_{int} > 1$M), f_{occ} saturates to the value $f_{occ} = 0.9$. Perhaps the most noticeable discrepancy is in $\tilde{p}_8$, the probability that all three sites (S_{int}, S_{cen}, and S_{ext}) are occupied. In the 8-state model, this saturates to a value of ca. 0.6, whereas in the multi-ion continuous space model it saturates to ca. 0.5, that is, there is a roughly 20% discrepancy between the two results. This degree of fractional error typifies comparisons between the models. Indeed, looking at the continuous space steady-state distribution of ions in the multi-ion model of ref 1, we find that up to 15% of the ions residing in the channel interior cannot be ascribed to any of the 3 binding sites. This provides one measure of quantification of the degree to which the multi-ion continuous space BD model can *not* be mapped to an eight-state discrete model: small but nonzero.

Given the steady-state probability distributions summarized above, we can easily calculate the average open-gate times and the rate of ion permeation through the open channel by processing this probability distribution data as discussed in Section IV. Adopting the gate particle potential $\phi_g(\theta)$ corresponding to parameter set 6 of ref 1, the discrete-state model result for the gate open time as a function of internal Cl^- concentration at a fixed external Cl^- concentration of 0.135 M is shown via the black solid line in Figure 7. The corresponding result for the situation where the internal concentration of Cl^- is fixed at 0.135 M, and the external concentration is varied is shown via the red line. These curves should be compared with corresponding results obtained via full multiparticle BD simulation (see Figure 7 of ref 1), which are shown via filled diamond symbols in the same figure. The agreement between corresponding predictions is quite reasonable (typically within ∼20%) given the inherent approximations involved in the reduction of multiparticle motion in continuous 3D space to an 8-state discrete-state linear kinetic scheme. Note that the dependence

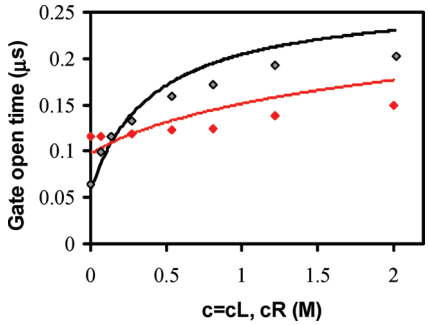

Figure 7. Average gate open times obtained from the 8-state kinetic model (solid lines) and multi-ion 3D BD model (filled diamonds) for the gate particle potential designated as parameter set 6 in ref 1: black shows dependence on $[Cl^-]_{int} = cL$ when $[Cl^-]_{ext} = 0.135$ M; red shows dependence on $[Cl^-]_{ext} = cR$ when $[Cl^-]_{int} = 0.135$ M. The error bars for the BD simulations are ±10%.

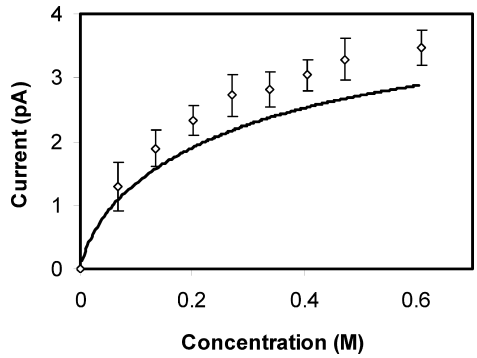

Figure 8. Ion current vs $[Cl^-]_{int}$ for fixed $[Cl^-]_{ext} = 0.135$ M at $V_{ap} = -100$ mV obtained from 8-state kinetic model (solid line) and from multi-ion 3D BD model (open diamonds with error bars).

of the gate open time on $[Cl^-]_{ext}$ at fixed $[Cl^-]_{int}$ is weaker than the dependence of the gate open time on $[Cl^-]_{int}$ at fixed $[Cl^-]_{ext}$, as observed experimentally in ClC-0 channels.[38,39]

The prediction of the 8-state discrete model for the dependence of ion current through the open-state ClC channel on $[Cl^-]_{int}$ at fixed $[Cl^-]_{ext} = 0.135$ M and applied transmembrane voltage of −100 mV is shown in Figure 8. The analogous results for this current-concentration (I−C) curve obtained via the multi-ion BD simulation model of ref 1 are shown in the same figure. Again, the overall agreement is good, with discrepancies of <20% between corresponding data points.

VI. Discussion and Conclusions

The permeation dynamics of ions moving through a ClC ion channel and the coupling of this motion to the closing of the fast gate of this channel constitutes a complicated interacting many-body problem that takes place in continuous 3D space and on long time scales. In ref 1 we constructed a coarse-grained model of this process and carried out 3D BD simulations of it. These simulations, while providing useful insights into the underlying dynamical process (time scales, ion fluxes, and mechanisms), strain the limits of our current computing capacity and must be painstakingly repeated each time a parameter in the model is changed (e.g., applied voltage, depth of an ion binding site within the channel, ionic strength of the bathing solutions, etc.). Thus, it is gratifying that we were able to map this complex kinetic process to an eight-state discrete model with dynamics governed by the linear kinetic master equations specified in eq 6, with a relatively sparse set of nonzero state-to-state rate constants. Furthermore, we successfully utilized a divide and conquer strategy wherein the rate constant for each nonzero pairwise state-to-state transition was computed via an appropriate 3D BD simulation procedure for a chosen applied transmembrane voltage and bathing solution concentration. Given numerical values for these rate constants, it was possible to carry out time evolution of various kinetic process via eq 6 to arbitrary long times, and, in particular, to extract the current of Cl^- ions through the channel in its open-pore conformation as well as the average time for the fast gate to close, as a function of Cl^- concentration in the intracellular and extracellular reservoirs. Good agreement with direct 3D BD simulation of the multi-ion process was obtained.

It would be useful to have a simpler way to compute the required state-to-state rate constants, one which could be quickly recalculated when the single ion PMF or other system parameters are modified. For the site-to-site hopping rate constants, the Kramers theory of one-dimensional activated barrier crossing processes immediately comes to mind. The state-to-state transition process of interest is in this case a single-ion barrier crossing event. In fact, the ion is moving in 3D, in the cylindrical pore region of the channel. However, since in our model the radius of the channel is taken to be constant over the interval between the location of the initially occupied binding site (potential well minimum) and the transition state (barrier height maximum), the geometrical details in the transverse directions are irrelevant: they cancel out of the final result for the hopping rate constant, which, again, is given by the well-known high-friction Kramers formula:

$$k_{hop} = \beta D \frac{\sqrt{\kappa_w \kappa_b}}{2\pi} \exp(-\beta E_a) \qquad (10)$$

Here, κ_w is the second derivative (curvature) of the single-ion PMF evaluated at the local minimum corresponding to the initial binding site, while κ_b is the negative of the second derivative of the PMF evaluated at the local maximum; furthermore, E_a is the activation energy for the process (the energy of the barrier top relative to the bottom of the initial binding site well).

As an example, let us consider the rate constant k_{34}, which describes hopping from S_{cen} to S_{ext}. If the channel is otherwise empty (no Cl^- in S_{int}), then the relevant single ion PMF is shown in Figure 4 (blue dashed line). This is the same single ion PMF used in the 3D BD simulations of ion permeation through the channel. To calculate the hopping rate from S_{cen} to S_{ext}, we appeal to eq 10. In particular, we compute the PMF curvature at S_{cen} (i.e., κ_w) and the curvature at the maximum barrier height separating the S_{cen} and S_{ext} wells (this is $-\kappa_b$). Next, we need to assess the activation energy (PMF at the barrier maximum minus PMF at the S_{cen} well). Finally, we note that the relevant diffusion constant for all site−site hopping processes within the channel is $D = 20$ Å^2/ns.[1] Plugging these parameters into eq 10 gives $k_{34} = 0.528$ ns^{-1}, in good agreement with the value of 0.525 ns^{-1} obtained from 3D BD simulation. There are a total of four state-to-state constants in the model (including k_{34}) that involve hopping between S_{cen} and S_{ext}, plus four state-to-state rate constants in the model which involving hopping between S_{int} and S_{cen}.

Calculation of the remaining 16 nonzero state-to-state rate constants, which involve either influx of an ion from a reservoir into one of the exterior sites into channel, or the reverse, efflux process, is more involved. The efflux process involves only one particle, so it can be analyzed via a single particle 3D Smoluchowski equation, but the geometry is more complicated than the simple 1D collinear motion relevant to internal site-to-site hopping dynamics. The influx process is more compli-

cated still. At low bathing solution concentrations, the ions in the bulk reservoir move independently of each other and thus a single particle 3D Smoluchowski equation is appropriate. Such an analysis necessarily predicts that the influx rate constant increases proportionally to the bathing solution concentration of Cl^-. However, as we learned upon conducting full multi-ion BD simulations of this process including ion−ion interactions, such behavior is not found except at very low ionic strengths of the bathing solution (cf. Figure 5). In the experimentally relevant range of these ionic strengths, the influx rate constant increases *sub*linearly with bulk [Cl^-] concentration, reflecting ion−ion repulsions between Cl^- ions entering into the channel vestibule. Clearly, analysis of these influx rate constants is challenging and would make an interesting subject for further research. Also of interest would be to include gate protonation/deprotonation processes in the model, since the protonation state of the glutamate fast gate appears to play a critical role in the operation of the channel.[36,37,40,41] This will of course modify the PMFs experienced by the permeating ions to reflect, among other things, addition or deletion of fixed charge on the gate moiety. The expandability of discrete-state models to include further mechanistic components underlying the overall kinetic process is a strength which we hope to exploit in future work.

Acknowledgment. We gratefully acknowledge financial support from the NSF (CHE-0518044 and CHE-0750332), and computational support from the Center for Molecular and Materials Simulation (CMMS) at the University of Pittsburgh.

References and Notes

(1) Cheng, M. H.; Mamonov, A. B.; Dukes, J. W.; Coalson, R. D. *J. Phys. Chem. B* **2007**, *111*, 5956.
(2) Zhou, Y.; Pearson, J. E.; Auerbach, A. *Biophys. J.* **2005**, *89*, 3680.
(3) Coalson, R. D. *J. Phys. A: Math. Theor.* **2008**, *41*, 115001.
(4) Grabe, M.; Bichet, D.; Qian, X.; Jan, Y. N.; Jan, L. Y. *Proc. Natl. Acad. Sci. U.S.A.* **2006**, *103*, 14361.
(5) Hlavacek, W. S.; Faeder, J. R.; Blinov, M. L.; Posner, R. G.; Hucka, M.; Fontana, W. *Sci. STKE* 2006.
(6) Wales, D. J. *Energy Landscapes: With Appications to Clusters, Biomolecules and Glasses*; Cambridge Univ. Press: Cambridge, 2003.
(7) Bernèche, S.; Roux, B. *Proc. Natl. Acad. Sci. U.S.A.* **2003**, *100*, 8644.
(8) Yang, J.; Monine, M. I.; Faeder, J. R.; Hlavacek, W. S. *Phys. Rev. E Stat. Nonlin. Soft Matter. Phys.* **2008**, *78*, 031910.
(9) Lu, D.; Grayson, P.; Schulten, K. *Biophys. J.* **2003**, *85*, 2977.
(10) van Kampen, N. *Stochastic Processes in Physics and Chemistry*; North Holland: Amsterdam; New York, 1992.
(11) Zwanzig, R. *Nonequilibrium Statistical Mechanics*; Oxford Univ. Press: 2001.
(12) Gillespie, D. T. *J. Phys. Chem.* **1977**, *81*, 2340.
(13) Henkelman, G.; Jonsson, H. *J. Chem. Phys.* **2001**, *115*, 9657.
(14) Chan, H. S.; Bromberg, S.; Dill, K. A. *Philos. Trans. R. Soc. Lond. B. Biol. Sci.* **1995**, *348*, 61.
(15) Zwanzig, R. *Proc. Natl. Acad. Sci. U.S.A.* **1997**, *94*, 148.
(16) Privalov, P. L. *Adv. Protein Chem.* **1979**, *33*, 167.
(17) Wales, D. J. *Int. Rev. Phys. Chem.* **2006**, *25*, 237.
(18) Hille, B. *Ion Channels of Excitable Membranes*, 3rd ed.; Sinauer Assoc., Inc.: Sunderland, 2001.
(19) Engh, A. M.; Faraldo-Gomez, J. D.; Maduke, M. *J. Gen. Physiol.* **2007**, *130*, 335.
(20) Engh, A. M.; Faraldo-Gomez, J. D.; Maduke, M. *J. Gen. Physiol.* **2007**, *130*, 351.
(21) Dutzler, R.; Campbell, E. B.; Cadene, M.; Chait, B. T.; MacKinnon, R. *Nature* **2002**, *415*, 287.
(22) Dutzler, R.; Campbell, E. B.; MacKinnon, R. *Science* **2003**, *300*, 108.
(23) Miloshevsky, G. V.; Jordan, P. C. *Biophys. J.* **2004**, *86*, 825.
(24) Cohen, J.; Schulten, K. *Biophys. J.* **2004**, *86*, 836.
(25) Faraldo-Gomez, J. D.; Roux, B. *J. Mol. Biol.* **2004**, *339*, 981.
(26) Bostick, D. L.; Berkowitz, M. L. *Biophys. J.* **2004**, *87*, 1686.
(27) Gervasio, F. L.; Parrinello, M.; Ceccarelli, M.; Klein, M. L. *J. Mol. Biol.* **2006**, *361*, 390.
(28) Corry, B.; O'Mara, M.; Chung, S. H. *Biophys. J.* **2004**, *86*, 846.
(29) Bisset, D.; Corry, B.; Chung, S. H. *Biophys. J.* **2005**, *89*, 179.
(30) Graf, P.; Nitzan, A.; Kurnikova, M. G.; Coalson, R. D. *J. Phys. Chem. B* **2000**, *104*, 12324.
(31) Cheng, M. H.; Cascio, M.; Coalson, R. D. *Biophys. J.* **2005**, *89*, 1669.
(32) Mamonov, A. B.; Kurnikova, M. G.; Coalson, R. D. *Biophys. Chem.* 2006.
(33) Berg, H. C. *Random Walks in biology*; Princeton University Press: Princeton, 1993.
(34) Cheng, M. H.; Coalson, R. D. *J. Phys. Chem. B* **2005**, *109* (1), 488.
(35) Graf, P.; Kurnikova, M. G.; Coalson, R. D.; Nitzan, A. *J. Phys. Chem. B.* **2004**, *108*, 2006.
(36) Dutzler, R. *FEBS Lett.* **2007**, *581*, 2839.
(37) Miller, C. *Nature* **2006**, *440*, 484.
(38) Chen, T. Y.; Miller, C. *J. Gen. Physiol.* **1996**, *108*, 237.
(39) Chen, T. Y.; Chen, M. F.; Lin, C. W. *J. Gen. Physiol.* **2003**, *122*, 641.
(40) Wang, D.; Voth, G. A. *Biophys. J.* **2009**, *97*, 121.
(41) Lisal, J.; Maduke, M. *Nat. Struct. Biol.* **2008**, *15* (8), 805.

JP907965B